Supplementary Information for "Reduced graphene oxide as a thin film electronic material"

1. Oxidation of graphite

Graphite oxide was prepared using modified Hummer's method[S1]. A mixture of 5 g of Graphite (SP-1 graphite, Bay Carbon) and 3.8 g of $NaNO_3$ was placed in a flask cooled in an ice bath. 169 mL of H_2SO_4 was added to the mixture and stirred until homogenized. 22.5 g of $KMnO_4$ was gradually added to the solution over 1 hour while stirring. The solution was removed from the ice bath after 2 hours, and was further stirred for 5 days. Brown-colored viscous slurry was obtained after 5 days. The slurry was added to 500 mL aqueous solution of 5 wt% H_2SO_4 over 1 hour while being continuously stirred. The mixture was stirred for further 2 hours. H_2O_2 (30 wt% aqueous solution) was then added to the mixture and stirred for further 2 hours.

The mixture was purified by dispersing and precipitating the above mixture in 500 mL aqueous solution of 3 wt% H_2SO_4 and 0.5 wt% H_2O_2. After two days of precipitation, supernatant solution was removed. This process was repeated ten times. 0.5 mL of the slurry was then dispersed in 500 mL of deionized water by ultrasonication to achieve a clear yellow suspension of exfoliated graphene oxide (GO). GO is soluble in water due to the presence of carboxyl and hydroxyl groups, allowing it to readily exfoliate in water. The suspension was allowed to stand for more than a month to allow precipitation of residual impurities. Supernatant of this suspension was found to be extremely stable for extended period of time without further precipitation. This parent suspension was diluted to different degree and used for further study.

The concentration of the resultant GO suspension was determined by first determining the concentration of GO in the slurry. A known amount of slurry was dried over P_2O_5 for 1 week in a

vacuum dessicator. From the weight of the dry GO product, the concentration of GO in the slurry was found to be 49 mg/mL. The concentration of the above mentioned supernatant suspension of GO was estimated by monitoring the change in absorbance over the precipitation period. This yielded a value of 12.5 mg/L.

The GO flakes in the suspension are irregularly shaped and therefore specific lateral dimensions are difficult to obtain, however, our AFM, SEM and optical microscopy analysis yield a size range of 200 nm – 20 μm. Detailed atomic force microscopy analysis reveal empirical observations that small flakes are less defective while tears and folded over regions are readily visible on larger sized flakes. We are presently conducting a detailed analysis of the structural properties of the GO sheets in the suspension.

2. Vacuum filtration

The GO suspension obtained was vacuum-filtrated through a mixed cellulose ester (MCE) membrane (Millipore) with 25 nm pores. Controllable deposition of uniform layers can be achieved by either varying the filtration volume or the concentration of GO in the suspension. Doubling the concentration has the same effect as doubling the filtration volume. The effective filtration volume in the manuscript refers to the volume of 0.33 mg/L suspension required to achieve the mass deposited by suspension of other concentrations.

Since individual sheets of GO are sufficiently larger than the pore dimension, growth occurs by creating a uniform continuous thin film of a single layer first and then by building additional layers on top. During filtration, as one pore becomes clogged, the permeation through the adjacent pore is enhanced until it is closed by a GO sheet and the process continues until a uniform layer is obtained. Once a continuous monolayer of graphene sheet is obtained, the deposition of additional layers is hampered due to a dramatic reduction in the permeation rate. Since the pores are not uniformly

distributed on the filter membrane and the GO sheets are irregularly shaped with a distribution in sizes, several sheets from several nearby pores can overlap, giving rise to regions consisting of 3-5 layers among single monolayer as shown in Figure 1d.

The GO films were transferred onto a variety of substrates such as glass, SiO2 on Si, Si, PET, ITO and metal films. The process is highly repeatable and the GO films, like the SWNT thin films deposited in our laboratory, are free of substantial defects such as delaminated regions and generally sufficiently well adhered to allow lithographic processing. Successful GO transfer on rough surfaces such PET with average roughness values of tens of nanometers was achieved. However, a detailed study on the effect of surface morphology on the transfer process is required and is underway in our laboratory.

3. Chemical reduction

The GO thin films were reduced using saturated vapor of dimethylhydrazine[S2]. Substrates were placed in a loosely sealed petri dish in which a reservoir of 1 vol% aqueous solution of dimethylhydrazine in a smaller petri dish was prepared. The petri dish was heated to 80 ^{o}C on a hot plate for 24 hours. The substrates were allowed to dry in air after this process for at least 1 hour. Further reduction was conducted by annealing the films in nitrogen environment or in vacuum for 5 hours at 200 ^{o}C. The XPS data in Figure S1 shows depression of C-O, C=O and C(O)O peaks with respect to C-C peak in each reduction step. These changes are in agreement with previous studies on the reduction of graphene oxide[S3, 4].

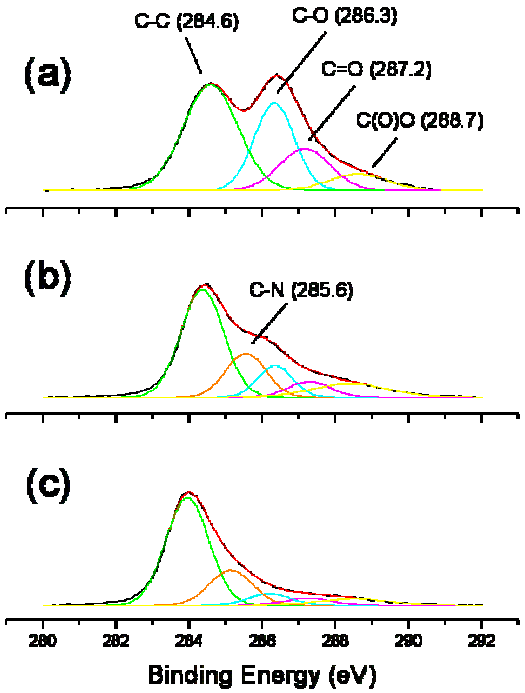

Figure S1 – C1s XPS spectra for (a) GO, (b) reduced GO, and (c) reduced and annealed GO. Peaks corresponding to different carbon bonds are indicated.

4. Atomic Force Microscopy

The morphology of reduced GO films was studied using AFM (Nanoscope IV, Digital Instruments). Height profiles were obtained in tapping mode. Probes used for this study had a force constant = 40 N/m and tip curvature <10 nm. Figure S2 shows the height image with height profiles. For 20 mL films, step height at the edges of individual flake was examined. Step height of most flakes for 20 mL films were found to be between 1 and 2 nm (Figure S2(b)), corresponding to 1 to 2 layers of GO. In order to study the thickness of 80 mL films, scratches were introduced in the films using sharp forceps. Height profiles were obtained at the edges of these scratches. The film thickness of the 80 mL samples were found to be between 3 to 4 nm corresponding to 3 to 5 layers of GO.

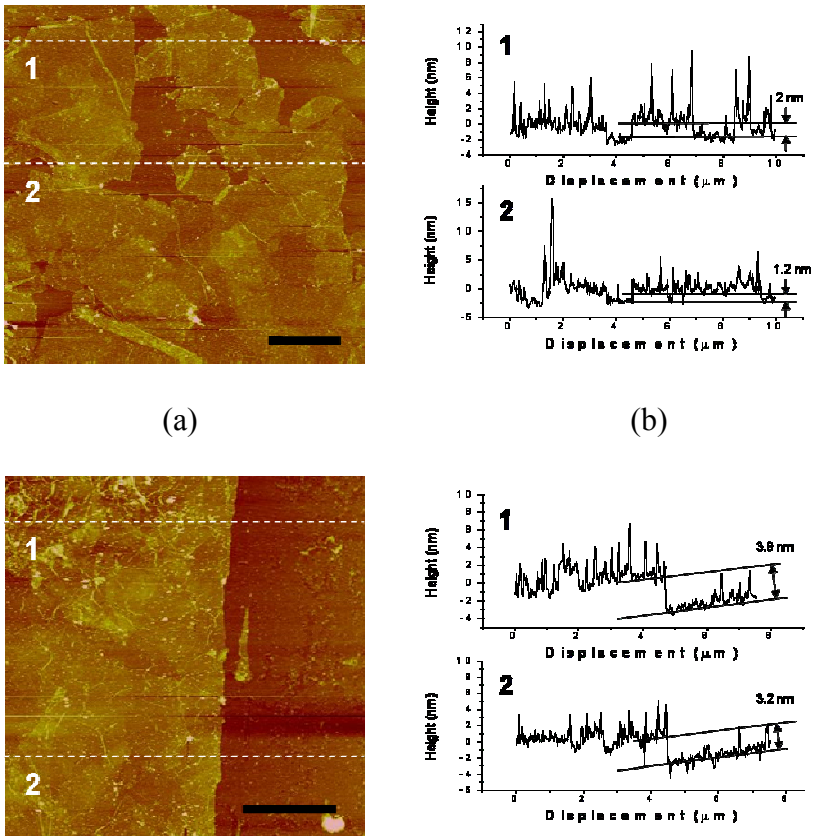

(a) (b)

(c) (d)

Figure S2 – AFM images of reduced and annealed GO thin films. (a) and (c): height images of 20 and 80 mL GO films. (b) and (d): line scans for 20 and 80 mL films along the dashed lines on the height images in (a) and (c). The scale bar in the images corresponds to 2 μm.

5. Scanning Electron Microscopy

Reduced and annealed GO thin films were also examined using scanning electron microscope (Sirion, FEI company). Samples were prepared on Si substrates with thermally grown oxide of 300 nm. Contrast can be observed between conducting GO films and the insulating substrate, indicating the presence of uncovered regions between the GO sheets. Figure S3 shows changes in the film

coverage on substrate surface with different filtration volumes. The SEM images suggest that continuous layer is achieved at filtration volumes > 70 mL, consistent with the sheet resistance data.

Deposition of thin films below 80 – 120 mL leads to the presence of uncovered regions between the reduced GO sheets. The fraction of which gradually decreases with filtration volume (Figure S3). Although conduction amongst the graphene sheets occurs even at very low filtration volumes, the number conducting channels is limited and thus the films have high sheet resistance. As the filtration volume is increased up to a critical value, the voids are filled and the overlapping of sheets becomes prevalent which leads to an increase in the number of lateral conduction channels. The reduction process may be only effective for uppermost layers, in which case only those layers that are reduced contribute to electrical conduction.

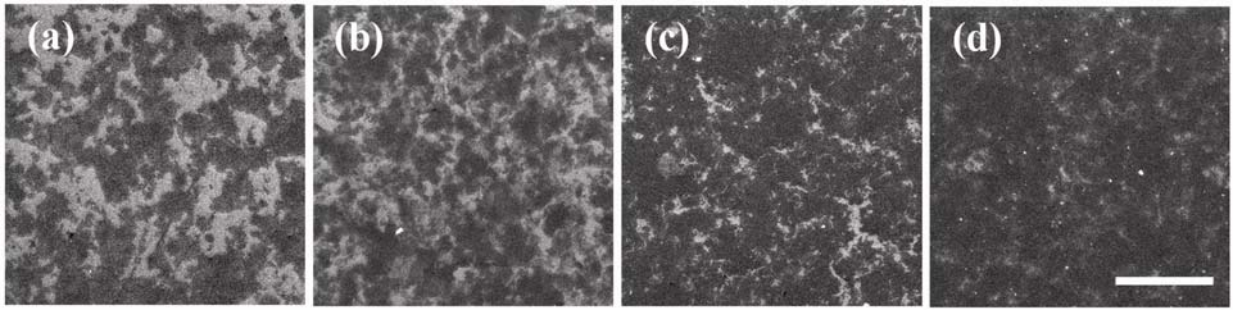

Figure S3 – SEM images of reduced and annealed GO thin films with different filtration volumes: (a) 20 mL (b) 30 mL, (c) 50 mL, (d) 70 mL. The scale bar corresponds to 20 μm.

6. Raman spectroscopy

The entire Raman spectra for a single- and multi-layered reduce GO regions are presented in Figure S4. The three major carbon features (*D*, *G* and *2D* peaks) along with the Si peaks from the substrates are labeled. The prominent *D* peak in the Raman spectra is an indication of the presence of disorder in the samples as previously discussed[S3, 5]. This is likely related to both the structural

disorder induced by the tears and folding over of the reduced GO sheets as well as the presence of residual oxygen and point defects[S6]. The *2D* peaks intensities have been enlarged ten times in order to demonstrate the shift between the single- and multi-layered regions.

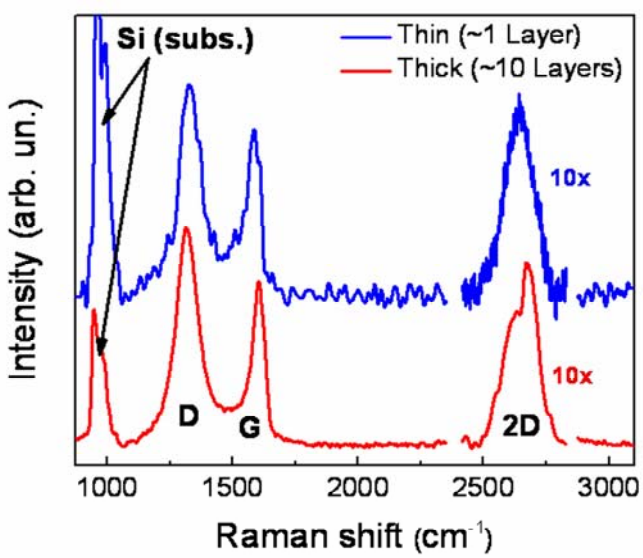

Figure S4: Raman spectra for a single- and ten-layered reduced GO regions.

The results of Raman mapping for the 50 mL sample indicate that it consists predominantly of 2 layered graphene as shown in Figure S5a. The powerfulness of Raman mapping, compared to optical images, in distinguishing thick and thin graphene, broadly corresponding to the lower left and upper right corners of the optical image, is evident from Figure S5b.

No. of layers	f(2D) @633 nm (cm^{-1}) Ref. 33	$F(2D)_{min}$ (cm^{-1})	$f(2D)_{max}$ (cm^{-1})
1	2640	-	2645.0
2	2650	2645.0	2657.5

3 to 5	2675	2657.5	2680.0
> 6	2685	2680.0	-

Table SI: 2D peak sheets as a function of number of graphene layers.

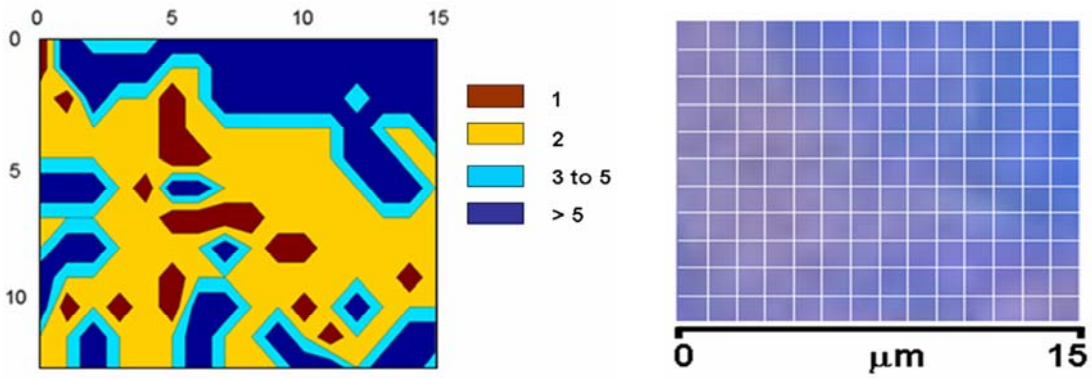

(a) (b)

Fig S5 – (a) A Raman map of a reduced GO thin film produced at a filtration volume of 50 mL. (b) Optical image showing the same area of the 50 mL sample which demonstrates the powerfulness of Raman mapping in distinguishing thick and thin graphene (broadly corresponding to the lower left and upper right corners of the optical image, respectively). The matrix of points used to record the Raman map correspond to the white grid in panel.

7. Spectroscopic Ellipsometry

Spectroscopic ellipsometry data were recorded in the Visible/Near-UV photon energy range (2.0-6.5 eV) using a Jobin-Yvon UVISEL ellipsometer at 70^{O} incidence angle from samples deposited on glass (20 to 80 mL, 10 mL step, both as prepared, reduced and reduced-annealed). The light spot size was about 1 mm in diameter. The as-recorded ellipsometer angles, Ψ and Δ, were modeled using the classical (Drude-Lorentz) model for semimetals. Although varying for each of the three sets of samples (as prepared, reduced and reduced-annealed) the optical constants of

graphene thin films were assumed to be the same for samples at different filtration volumes, expected to have variable thicknesses and fraction of voids. Globally fitting each of the three sets of data we were able to obtain, for each, its complex refractive index (Figures S6a and S6b) and the variations in thickness and fraction of voids with the filtration volume, which agree well with the values previously estimated from the AFM, Raman map and SEM images (Figures S2, S3, and S5).

From the extinction coefficients (i.e. the imaginary parts of the complex refractive indices) in Figure S6b it can be inferred that the optical absorption of all these samples is dominated by π-π* transitions, which generally give rise to an absorption peak at 4.5-5.5 eV[S7], while the contribution of conduction electrons is minimal in the Visible/Near-UV photon energy range. It can also be noticed that the π-π* peak intensity is relatively low for as prepared graphite oxide, whilst increasing both with reduction and annealing. This effect, which can be related to ordering[S7], may be responsible to the decrease in transmittance of the films. Annealing also considerably downshifts the peak energy for π-π* transitions, an effect sometimes attributed to the coalescence of ordered graphitic islands[S7].

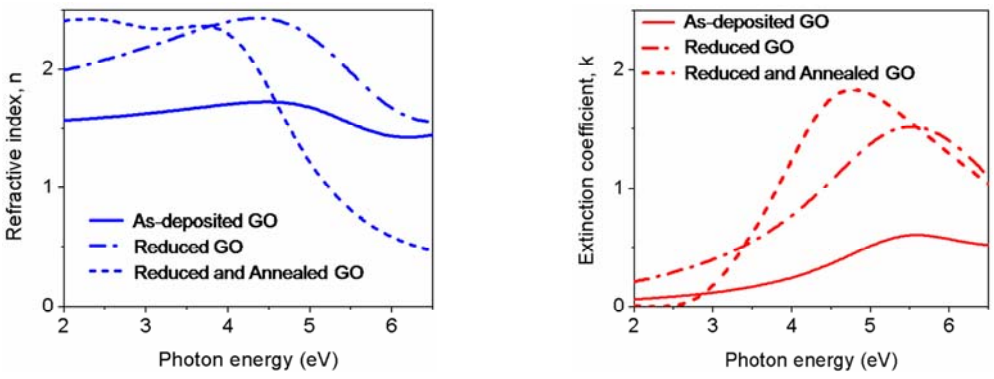

(a) (b)

Fig S6 – Optical constants determined by spectroscopic ellipsometry: (a) real and (b) imaginary part of the complex refractive index.

8. Film transparency

Transmittance of the graphene thin films was obtained in visible wavelength range using UV-visible absorption spectrometer (S2000-UV-VIS, Ocean Optics, Inc). Transmittance showed monotonous decrease with increasing photon energy as shown in Figure S7a. Transmittance was measured before and after each reduction steps. As film conductivity increased with reduction, transmittance was reduced significantly due to increased number π electrons as shown in Figure S7b.

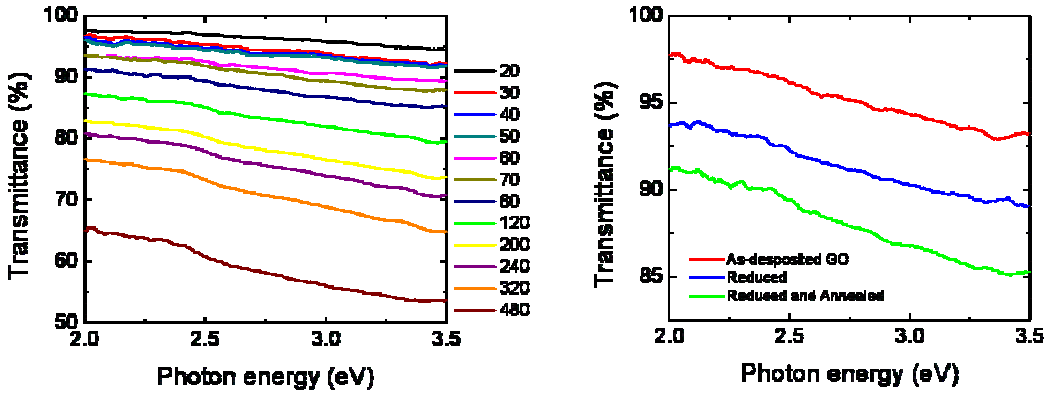

(a) (b)

Fig S7 – Transmittance as a function of photon energy. (a) Reduced and annealed GO films with different filtration volumes. (b) Changes in transmittance upon reduction and annealing for 80 mL films.

9. Organic photovoltaic devices

In order to use reduced GO thin films as the transparent and conducting electrode of organic solar cells, a 480 mL film was doped with Cl by dipping in thionyl chloride ($SOCl_2$) for 1 hour prior to deposition of the polymer layers. The resistivity typically decreased by a factor of up to 4 upon this treatment (See below). Organic solar cells were prepared by first depositing a layer of poly(3,4-ethylene dioxy-thiophene):poly(styrenesulfonate) (PEDOT:PSS) on top of the reduced and doped

GO film by spin-coating at 4500 rpm. A 1:1 weight ratio mixture of poly(3-hexylthiophene)(P3HT) and phenyl-C61-butyric acid methyl ester (PCBM) was prepared at a concentration of 20 mg/L and spin-coated over PEDOT:PSS layer at 700 rpm. P3HT was developed in Profs. Su and Chen's group at Natonal Taiwan University and was found to have molecular weight of 58,178 g/mol, polydispersity index of 1.62, and regioregularity of 96 %. The results of a proof of concept OPV device with Cl doped graphene electrode are shown in Figure S8. The efficiency of the reduced GO electrode device is ~ 0.1% which is substantially lower than that of state-of-the-art indium tin oxide (5.5%)[S8] and SWNT thin films (2.5 %)[S9] OPV devices.

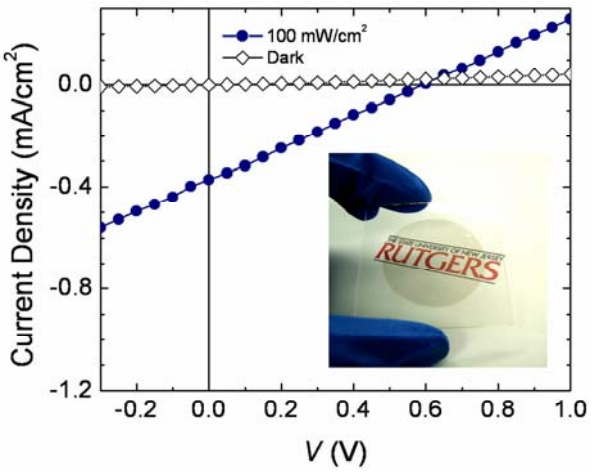

Figure S8– I-V characteristics of OPVs under no illumination and under one sun illumination (100 mW/cm^2). Inset is a photograph of the reduced graphene thin film used for the OPV fabrication.

We now describe the chlorine doping process which leads to an enhancement in sheet resistance. The decrease in sheet resistance at room temperature in air with Cl doping of reduced GO thin films deposited at seven different filtration volumes is shown in Figure S9. The plot shows ratio of sheet conductance of Cl doped to undoped thin films from two different batches. It can be seen that sheet conductance increased by a factor of 2 – 6 after exposure to $SOCl_2$.

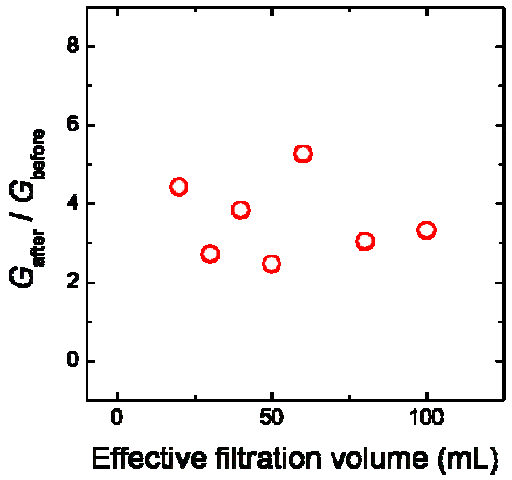

Figure S9: Ratio of the sheet conductance after $SOCl_2$ exposure to reduced GO thin films. It can be seen that the conductance increases by 2 – 6 times via Cl doping.

In order to confirm that exposure to $SOCl_2$ does indeed lead to doping, we have carried out TFT measurements at low temperatures on 50 mL film. From Figure S10, it can be seen that the conductance of $SOCl_2$ exposed films can be modulated by the gate voltage. Furthermore, the effect is similar to the oxygen and vapor doping effect[S10, 11] with the crucial difference that it persists in vacuum and low temperature. It can be seen in Figure S10 that the conductance of the Cl exposed films is always higher and clear p-type device characteristics are observed for the measurements in vacuum and at 4.2 K.

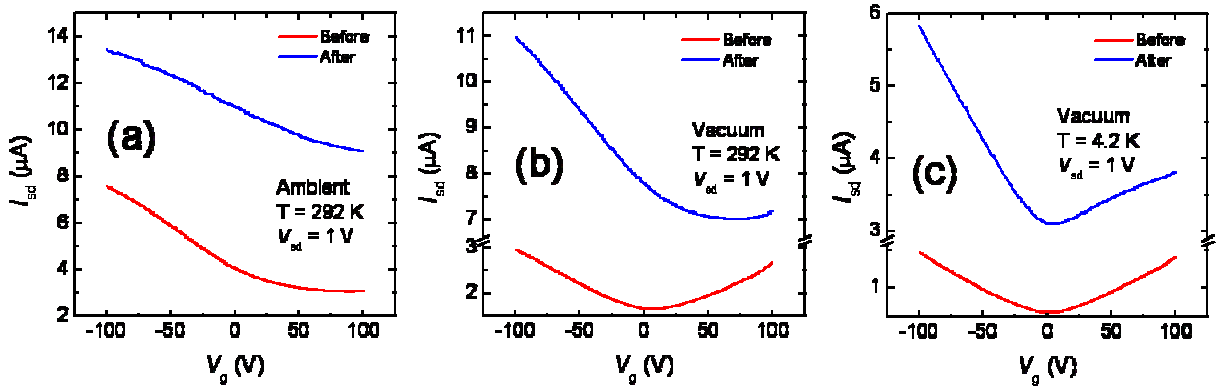

Figure S10 – Transfer characteristics of Cl doped 50 mL reduced GO films (a) in ambient condition, (b) in vacuum at room temperature, and (c) in vacuum at liquid Helium temperature.

It should be noted that our Cl doping work was intended to enhance the conductance of the reduced GO thin films so that OPVs could be fabricated. However, further investigation is merited since the electrodes are semi-conducting rather than conducting. A thorough analysis of the data will be conducted and a detailed study will be reported elsewhere.

10. Obtaining mobility from TFT

The mobility values were extracted from the TFT transfer characteristics by commonly used equation below.

$$\mu = \frac{L}{WC_{ox}V_{sd}} \frac{\Delta I_{sd}}{\Delta V_g}$$

Here, L and W are the channel length and the width, C_{ox} is the gate oxide capacitance, V_{sd} is the source-drain voltage, I_{sd} is the source-drain current, and V_g is the gate voltage. Cox is $\varepsilon_{ox}\varepsilon_0/t_{ox}$, where ε_{ox} is the permittivity of the oxide, ε_0 is the permittivity of free space, and t_{ox} is the oxide thickness. $\Delta I_{sd}/\Delta V_g$ is the transconductance or the slope of the transfer curve in the linear regime as shown in Figure S11. When the measurements were performed in ambient conditions, the electron branch

was barely present and often times not observed within the investigated gate voltage range (See Figure S10a). It was therefore difficult to obtain the correct value of electron mobilities. Nevertheless, electron mobilities were obtained for cases when the electron branch was observed as in Figure S11. The hole and electron mobilities were found to be on the order of 1 and 0.2 cm^2/V-s respectively, and were generally higher for films with high conductivity. These mobility values are similar to some reports on SWNT networks[S12] but substantially lower than the state-of-the-art highly aligned SWNT network devices reported by the Rogers group[S13]. The mobility and the on/off ratio of the devices were found to be almost independent of the channel length within the investigated range.

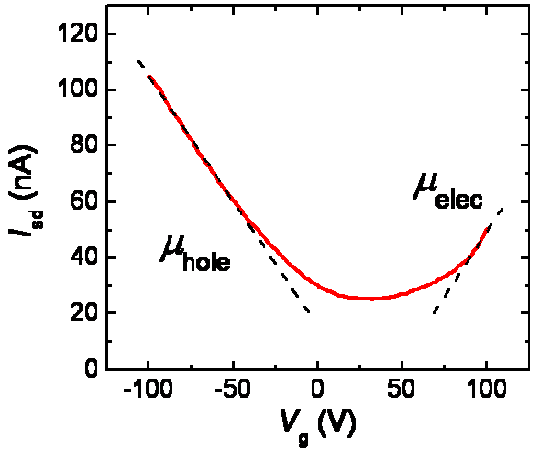

Figure S11 – An example of a linear fit for extracting device mobilities. Hole and electron mobilities were calculated from the respective branch.

References for Supplementary Information

S1. Hirata, M., Gotou, T., Horiuchi, S., Fujiwara, M. & Ohba, M. Thin-film particles of graphite oxide 1: High-yield synthesis and flexibility of the particles. *Carbon* **42**, 2929-2937 (2004).

S2. Stankovich, S. *et al.* Graphene-based composite materials. *Nature* **442**, 282-286 (2006).

S3. Stankovich, S. *et al.* Synthesis of graphene-based nanosheets via chemical reduction of exfoliated graphite oxide. *Carbon* **45**, 1558-1565 (2007).

S4. Watcharotone, S. *et al.* Graphene-silica composite thin films as transparent conductors. *Nano Lett.* **7**, 1888-1892 (2007).
S5. Gomez-Navarro, C. *et al.* Electronic transport properties of individual chemically reduced graphene oxide sheets. *Nano Lett.* **7**, 3499-3503 (2007).
S6. Schniepp, H. C. *et al.* Functionalized single graphene sheets derived from splitting graphite oxide. *J. Phys. Chem. B* **110**, 8535-8539 (2006).
S7. Robertson, J. Diamond-like amourhpous carbon. *Mater. Sci. Eng. R* **37**, 129-281 (2002).
S8. Li, G. *et al.* High-efficiency solution processable polymer photovoltaic cells by self-organization of polymer blends. *Nature Mater.* **4**, 864-868 (2005).
S9. Rowell, M. W. *et al.* Organic solar cells with carbon nanotube network electrodes. *Appl. Phys. Lett.* **88** (2006).
S10. Collins, P. G., Bradley, K., Ishigami, M. & Zett, A. Extreme oxygen sensitivity of electronic properties of carbon nanotubes. *Science* **287**, 1801-4 (2000).
S11. Novoselov, K. S. *et al.* Electric field effect in atomically thin carbon films. *Science* **306**, 666-669 (2004).
S12. Artukovic, E., Kaempgen, M., Hecht, D. S., Roth, S. & Gruner, G. Transparent and flexible carbon nanotube transistors. *Nano Lett.* **5**, 757-760 (2005).
S13. Kang, S. J. *et al.* High-performance electronics using dense, perfectly aligned arrays of single-walled carbon nanotubes. *Nature Nanotech.* **2**, 230-236 (2007).